Vibrational frequencies via total-energy calculations. Applications to transition metals

K.-M. Ho, C. L. Fu, and B. N. Harmon
Ames Laboratory—U.S. Department of Energy and Department of Physics, Iowa State University, Ames, Iowa 50011
(Received 15 September 1983)

The important longitudinal $(\frac{2}{3},\frac{2}{3},\frac{2}{3})$ vibrational modes in Mo, Nb, and bcc Zr as well as the H-point modes in Mo and Nb have been studied using the frozen-phonon approach. These entirely first-principles calculations involve the precise evaluation of the total crystalline energy as a function of lattice displacement and yield calculated phonon frequencies to within a few percent of the experimental values. Anharmonic terms are readily obtained and are found to be very important for causing the tendency toward the ω-phase instability in bcc Zr. The charge densities and single-particle energies obtained in the course of the calculations allow a detailed analysis of the electronic response to lattice distortions and the mechanisms causing phonon anomalies. The calculations also provide first-principles benchmarks at a few wave vectors where the validity of phenomenological models can be tested or their parameters determined.

I. INTRODUCTION

Measurements of phonon dispersion curves not only yield data useful for understanding the thermophysical properties of materials, but also provide information about the essential interatomic forces in solids. In metals the fundamental phenomena of conduction-electron screening is manifested in the dispersion curves, and by careful analysis one may gain basic knowledge concerning both the electronic screening of interionic forces and the strength of the electron-phonon interaction. For nearly-free-electron metals such as Na for which the change in total energy caused by a phonon distortion of the lattice can be accurately obtained using a pseudopotential and second-order perturbation theory, the calculations of the phonon dispersion curves seem reasonably well in hand.[1,2] However, for materials containing transition metals the same methods are less satisfactory, and although great progress has been made in the last ten years there is still no completely adequate first-principles method for obtaining the lattice dynamics of solids possessing d-like valence electrons.[3,4] The numerous anomalies found in the phonon dispersion curves and the observed lattice instabilities in many transition-metal compounds, especially those exhibiting high-temperature superconductivity, provide additional motivation for studying the lattice dynamics and interatomic forces in these materials. In this paper we use an entirely first-principles method (the so-called frozen-phonon method) to study the lattice dynamics of some prototypical transition metals. Our results, which we describe later in the paper, are encouraging and confirm that the frozen-phonon method is a powerful new tool for investigating the microscopic interactions in solids. A brief description of this work has already been published,[5] and another paper describing the extension of the method to include the calculation of interatomic forces by using the Hellmann-Feynman theorem has also been published.[6] Before giving the details of the method and our results, we first place them in perspective by briefly describing earlier approaches and models.

Within the harmonic approximation the first goal of theory is to obtain the changes in total crystalline energy accurately to second order in the atomic displacements. The traditional method as reviewed by Born and Huang[7] or Maradudin *et al.*[8] is to make a formal expansion of the energy to second order (or higher) and to treat the expansion coefficients (force constants) as adjustable parameters (empirically determined). This approach has kept its utility as an interpolation and fitting scheme for experimental data with which the phonon density of states can be calculated and the lattice contribution to the specific heat determined. However, it has frequently failed as a heuristic model since for many solids with long-range forces the number of parameters required for a good fit becomes excessive and obscures the physical implications. For understanding the microscopic mechanisms which determine the lattice dynamics it is preferable to have a first-principles approach. The first steps in this direction were taken about the time neutron-inelastic-scattering results became available and there developed the strong interplay between experiment and theory which has characterized the field of lattice dynamics ever since. The principle theoretical ideas that were developed utilized the dielectric approach, which involves the determination of the valence-electron screening using linear-response theory. This method forms the basis for calculations of the simple metals,[2,9] and is the foundation for lattice-dynamical models of covalent crystals.[10,11] It is formally correct for any crystal; but direct implementation of the method, which includes the precise evaluation of the dielectric matrix, has proved numerically difficult. If matrix elements are neglected (a serious approximation), the calculation is reduced to the determination of the bare susceptibility or response function, $\chi^0(q)$, which can be easily calculated,[12,13] and has been used frequently to locate nesting features of Fermi surfaces and to confirm the electronic nature of the corresponding observed phonon anomalies.[14–17] However, not all anomalies in the experi-

mental phonon spectra of transition metals can be identified with structures in $\chi^0(q)$,[18] and the magnitudes of those anomalies that have been associated with such peaks have not been determined for lack of accurate matrix elements. There have been more recent efforts to reformulate the method in terms of localized basis states which would be appropriate for d-band metals, and this has led to a greater emphasis on the role of charge-density distortions.[3,19] However, details of the self-consistent screening (exchange and correlation effects) as well as other technical problems continue to hinder the adoption of this method for first-principles calculations. The simplified models based on this rigorous formulation have focused on the charge-fluctuation component of the electronic screening,[20,21] and subsequent empirical models are able to fit the phonon dispersion curves of Nb with considerably fewer adjustable parameters than the Born—von Kármán model by including charge-fluctuation degrees of freedom.[22,23] Nevertheless the number of parameters is still disturbingly high, and there has been no good test to determine if the fluctuations predicted in these models have physical significance, or if they merely provide for a better fitting scheme.

A more recent reformulation of the theory,[24] motivated in part by the success of local-density theory in calculating the ground-state electronic structure of metals, has many appealing features and has been adopted using an empirical tight-binding band-structure method to give the most successful treatment of transition-metal lattice dynamics to date.[25] The idea is to calculate to second order the phonon-induced changes in the total energy when it is separated into a "band-structure" term consisting of the sum of one-electron eigenvalues and a term which includes both the so-called "double-counting" energy, arising from the Hartree and exchange-correlation parts of the potential, and the ion-ion energy. The second-order changes in the band-structure term are straightforwardly calculated from perturbation theory and give rise to many of the interesting features of the phonon spectra. The remaining second-order terms can be grouped together and interpreted as arising from the interaction of neutral objects so that only short-range forces come into play. In their brilliant execution of these ideas, Varma and Weber were able to reproduce the anomalous features in the phonon dispersion curves of the Nb-Mo series of alloys.[25] Their methods have since been applied successfully to other systems.[26—28] These calculations have confirmed the importance of states near the Fermi level in producing phonon anomalies and have helped to clarify the role played by the electron-phonon matrix elements in systems with localized (rather than plane-wave-like) orbitals. To expedite their calculations Varma and Weber considered only the band-structure term and used a set of first- and second-nearest-neighbor force constants as adjustable parameters to account for the additional short-range interactions. Since some anomalies in phonon spectra and lattice instabilities can depend on short-range interactions, it is desirable to go beyond simple parametrization and obtain first-principles understanding of these forces.

The new approach to lattice dynamics which we use in this paper involves the precise determination of the crystalline total energy as a function of the lattice displacements associated with a particular phonon. The method, which is commonly referred to as the frozen-phonon method, utilizes first-principles band-structure techniques to obtain the total energy for each frozen-in position of the lattice. The phonon frequency can then be obtained from the resultant potential-energy curve. Unlike previous methods, this method requires no experimental input to obtain the phonon frequency. The only approximations made are the local-density approximation[29] for evaluating the ground-state total energy and the Born-Oppenheimer approximation.[30] Information concerning phonon anharmonicity and possible lattice instabilities can also be obtained because of the nonperturbative nature of the calculations. This approach is complementary to the other methods since, for computational reasons, it is necessary to focus on a few particular modes and examine the microscopic response and trends among several systems, while other methods model the whole phonon spectrum at one time. Recently, successful applications of the frozen-phonon method have been reported for semiconductors[31—34] and simple metals.[35] The method has also been extended to calculate interplanar force constants from which entire dispersion curves along a particular direction may be obtained if the forces are mostly short ranged.[36,37] There have been several other significant studies making use of frozen-phonon ideas, but accurate total energies were not calculated.[38—43] In this paper, we give details for the application of the method in studying transition metals: We have performed frozen-phonon calculations for the longitudinal $(\frac{2}{3},\frac{2}{3},\frac{2}{3})$ phonon modes in Mo, Nb, and the high-temperature bcc phase of Zr as well as the H-point phonon modes in Mo and Nb. In general, we find that the frozen-phonon approach yields phonon frequencies within a few percent of the measured values. The only exception is the H phonon of Mo where severe Fermi-surface nesting causes renormalization (or many-body) effects to become significant.[44]

The motivation for studying the longitudinal $(\frac{2}{3},\frac{2}{3},\frac{2}{3})$ mode [abbreviated $\mathrm{L}(\frac{2}{3},\frac{2}{3},\frac{2}{3})$] and the H-point phonon in Nb, Mo, and Zr is the marked difference in the phonon spectra of these metals at these wave vectors. Figure 1 shows the phonon dispersion curves for the longitudinal (111) branch measured by inelastic-neutron-scattering experiments for Mo,[45] Nb,[46] and the high-temperature (1400-K) bcc phase of Zr.[47] For Nb the longitudinal (111) phonon branch exhibits a dip near the $(\frac{2}{3},\frac{2}{3},\frac{2}{3})$ position, whereas the same branch in Mo is flat near $(\frac{2}{3},\frac{2}{3},\frac{2}{3})$ but shows a dip at the zone boundary (point H). Of particular interest is the $\mathrm{L}(\frac{2}{3},\frac{2}{3},\frac{2}{3})$ phonon of bcc Zr. This element undergoes a phase transformation to the hcp structure as the temperature is lowered below $\sim$1100 K. However, there is a competing transformation to the so-called ω phase by alloying[48] or by the application of high pressure.[49,50] The atomic displacements for the bcc—to—ω-phase transition are in the same directions as the polarization vectors for the $\mathrm{L}(\frac{2}{3},\frac{2}{3},\frac{2}{3})$ phonon mode. The experimental phonon dispersion curves for the high-temperature bcc phase (Fig. 1) indicate a huge dip in the (111) longitudinal branch with the minimum at $(\frac{2}{3},\frac{2}{3},\frac{2}{3})$ and a corre-

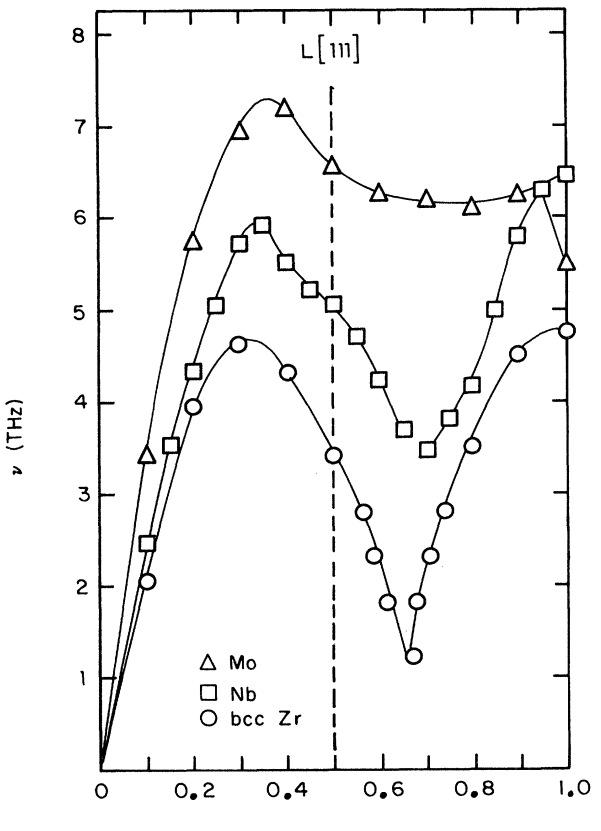

FIG. 1. Phonon dispersion curves for the longitudinal [111] branch measured by inelastic neutron experiment on Mo (Ref. 45) Nb (Ref. 46) and the high-temperature (1400-K) bcc phase of Zr (Ref. 47).

sponding peak in the quasielastic scattering at this wave vector suggesting an incipient lattice instability towards the ω phase. A similar dip at this wave vector has also been observed in the dispersion curves of the high-temperature bcc phase of La.[51]

This paper is organized as follows: Section II outlines the frozen-phonon method and contains the calculational details, Sec. III gives the results of the calculations, Sec. IV contains a more complete review of the bcc—to—ω-phase transformation as well as a discussion of the mechanisms responsible for the phonon anomalies, and Sec. V concludes the paper.

II. METHOD OF CALCULATION

A. Frozen phonons—concepts

In the Born-Oppenheimer[30] approximation, the motions of the ions are assumed to be so much slower than the motions of the electrons that at each instant the electrons are always in the ground state defined by the instantaneous ionic configuration. The total ground-state electronic energy, which is a function of the ionic positions, together with the potential from the ion-ion Coulomb interactions, yields a total potential for the ionic motions. It is this potential which is calculated in the frozen-phonon method. When the crystal is distorted with atomic displacements corresponding to a particular phonon mode having a wave vector commensurate with the bulk reciprocal lattice, the resultant deformed lattice can be viewed as a different crystal structure with reduced symmetry. The lowered symmetry usually implies a larger primitive unit cell and accurate calculations are limited by the total number of atoms per cell (about 10—15 atoms per cell is the maximum, but with newer programs and modern supercomputers this limitation is becoming less severe). With the atomic positions determined, an efficient band-structure program is used to obtain the ground-state total energy. It is essential that these calculations be self-consistent and that the program be able to treat general potentials (muffin-tin or other shape approximations to the potential can adversely affect the results). For numerical accuracy, the total energy is evaluated at displacements from equilibrium large enough for the change in total energy to be significant relative to the precision of the computer. Usually a number of displacements about equilibrium are chosen so that numerical consistency (or noise) can be monitored and anharmonic terms ascertained. If we restrict our consideration to small displacements we may consider only the second-order term and express the total energy per atom as

$$\Delta E_{\vec{q}} = \tfrac{1}{2} M \omega_{\vec{q}}^2 U_{0\vec{q}}^2 \frac{1}{N} \sum_i \cos^2(\vec{q}\cdot\vec{R}_i + \delta_{\vec{q}}) \, . \tag{1}$$

In this equation $\vec{R}_i$ is the equilibrium position of the ith atom, $U_{0\vec{q}}$ is the amplitude of the distorted wave, $\delta_{\vec{q}}$ is the phase factor, N is the number of atoms in the crystal, M is the atomic mass, and $\omega_{\vec{q}}$ is the phonon frequency.

For a zone-boundary phonon, Eq. (1) gives

$$\Delta E_{\vec{q}} = \tfrac{1}{2} M \omega_{\vec{q}}^2 U_{0\vec{q}}^2 \, , \tag{2}$$

and for a phonon mode of arbitrary $\vec{q}$ (except for zone-boundary phonons)

$$\Delta E_{\vec{q}} = \tfrac{1}{4} M \omega_{\vec{q}}^2 U_{0\vec{q}}^2 \, . \tag{3}$$

Thus from Eqs. (2) or (3), the phonon frequency can be evaluated from the curvature of the calculated energy-versus-displacement curve for small displacements. These results can be extended to the case of compounds and to general wave vectors where the lack of symmetry requires the calculation and diagonalization of the dynamical matrix to obtain the phonon frequencies and polarization vectors.

In the present study the calculations have been performed on monatomic bcc metals for the interesting phonons at L($\frac{2}{3},\frac{2}{3},\frac{2}{3}$) and the H point.

B. Geometry

1. $L(\frac{2}{3},\frac{2}{3},\frac{2}{3})$ phonon

In the presence of this phonon the distorted bcc crystal can be described by a unit cell consisting of three atoms. In Fig. 2(a), three neighboring atomic planes normal to the [111] direction of the bcc structure are shown, the phonon

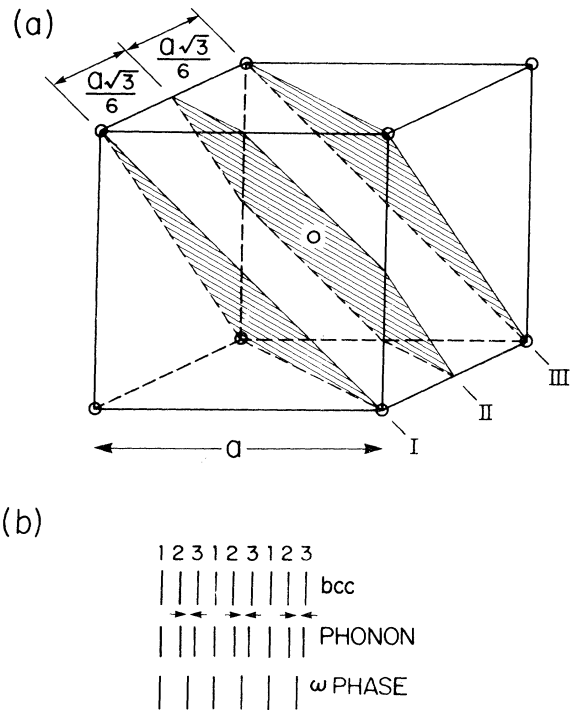

FIG. 2. (a) bcc lattice and three neighboring (111) planes. (b) Spacing of (111) planes in the bcc phase, the fully collapsed ω phase, and the phonon-distorted crystal pattern corresponding to the L($\frac{2}{3},\frac{2}{3},\frac{2}{3}$) phonon.

distortion corresponds to leaving every third plane (labeled plane 1) stationary and moving the remaining pair of adjacent planes (labeled planes 2 and 3) towards each other (or apart). When planes 2 and 3 collapse together as depicted in Fig. 2(b), the structure is known as the ω phase.

The distorted lattice can be described with a hexagonal primitive cell with $A=\sqrt{2}a$ and $C=(\sqrt{3}/2)a$, where a is the lattice constant of the bcc crystal and the C axis is along the (111) direction. The distorted crystal belongs to the trigonal system with space group $D^3_{3d}(P\bar{3}m1)$. For the ω phase, the space group is $D'_{6h}(P6/mmm)$. In our work we have kept the ideal C/A ratio of $\sqrt{3/8}=0.612$; however, measurements have indicated a slight distortion in the C/A ratio for the ω phase of Zr: 0.622.[52] We note that the ω-phase crystal structure can be obtained from the ZrB_2 structure[53] by simply replacing the boron atoms by Zr atoms.

2. *H-point phonon*

For this phonon the displacements have been chosen along the (100) direction. The primitive cell of the phonon-distorted lattice is simple cubic with two atoms, and the space group is $D^7_{4h}(P4/mmm)$ (nonsymmorphic).

C. $\vec{k}$-space sampling

Since the Brillouin zone of the phonon-distorted lattice is commensurate with that of the bulk bcc crystal, it is possible to choose a $\vec{k}$-point sampling grid common to both the distorted and undistorted bcc crystals when evaluating the eigenvalues and wave functions. This ensures a maximum cancellation of errors in subtracting energies to find the distortion energy. It is also essential that the grid for the distorted structure contain a complete set of $\vec{k}$ points so that the charge density regains the full cubic symmetry in the limit of zero distortion. This is not automatic when the electronic structure of the cubic crystal is calculated with the large unit cell containing three atoms and having hexagonal symmetry. Without this care in choosing $\vec{k}$ points, significant errors in the charge density and even unphysical charge transfers can be introduced at small displacements unless the number of $\vec{k}$ points sampled is made unnecessarily large.

Unlike the case with semiconductors where experience has shown acceptable convergence can be obtained with as few as 6 $\vec{k}$ points, the $\vec{k}$-point sampling in metals must be large enough to adequately account for the partial occupation of the bands crossing the Fermi level. Based on convergence studies we have used sets of uniform grid points in the present calculations: 57 $\vec{k}$ points within the irreducible wedge of the Brillouin zone (IBZ) for the L($\frac{2}{3},\frac{2}{3},\frac{2}{3}$) phonon and 126 $\vec{k}$ points in the IBZ for the H-point phonon. These particular grid points correspond to 55 and 112 $\vec{k}$ points, respectively, in the bulk bcc IBZ. For performing Brillouin zone sums it is necessary to carefully consider the weighting of those states with energies near the Fermi level. This is discussed further in the next section.

D. Calculational procedures

The calculations proceed in analogy to that of the bulk bcc structure,[54] except for the larger real-space unit cell and lower symmetry for the phonon-distorted structure. Our calculations were made using a first-principles pseudopotential method employing a mixed basis of plane waves and Gaussian functions which are included to ensure adequate convergence for the localized d-like orbitals.[55] The nonlocal ionic pseudopotentials are generated from first-principles atomic calculations according to the norm-conserving scheme of Hamann, Schluter, and Chiang,[56] and are the same as those used in the bulk calculations.[54] With these pseudopotentials the atomic valence-electron wave functions are reproduced exactly outside a core radius of about 2.3 a.u. for s-p—like states and about 0.8 a.u. for the d-like states. Thus the charge-density plots we show later should give an accurate representation of the actual valence charge density except in the small-volume region in the immediate vicinity of the nuclei. The Hedin-Lundqvist form of the local exchange-correlation potential was used.[57] The lattice constants used correspond to the calculated equilibrium values (3.460, 3.265, and 3.139 Å for bcc Zr, Nb, and Mo, respectively[54]). The cutoff energy ($E_C=10.5$ Ry) used to limit the plane-wave basis set to about 60 plane waves per atom, and the exponents of the Gaussian orbitals ($\lambda=1.30$, 1.20, and 1.12 a.u. for Mo, Nb, and Zr, respectively) also have the same values as used in the bulk calculations.

Several different schemes were attempted for weighting the $\vec{k}$ points near the Fermi level to account for the par-

tial occupation of the bands.[54] This is particularly important when considering distortions in metals so that the screening includes effects from the emptying of some states at the Fermi level and the filling of others. The scheme we found to be most effective was to broaden each energy level by a Gaussian whose width is chosen to be the same for all $\vec{k}$ points and is roughly equal to the dispersion of the energy bands between neighboring grid points near the Fermi level. The weight of each state is then determined by the portion of its Gaussian distribution which lies below the Fermi level. This scheme is easy to implement and in the cases we have tested it gave excellent convergence (see below and Ref. 54).

For small displacements ($\sim 1\%$ of the lattice constant) about equilibrium, the distortion energies involved are of the order 0.001 Ry per atom and numerical precision is extremely important. The calculations are feasible because we require only energy differences so that the major errors associated with the local-density approximation and $\vec{k}$-point sampling cancel in the subtraction. To insure that our calculations reach the desired level of precision we have made a number of convergence studies. Table I lists the results for the phonon frequency of the $L(\frac{2}{3},\frac{2}{3},\frac{2}{3})$ mode of Nb obtained from calculations with different numbers of sample grids and different values of the Gaussian smearing used in the Fermi-surface weighting. As mentioned above, the convergence is seen to be quite acceptable as long as the width of the Gaussian is well chosen. We have also carried out one calculation with a plane-wave cutoff energy of 14.5 Ry and a Gaussian orbital exponent of 1.25. The shift in the calculated phonon frequency was only 1%. Because nesting features of the Fermi surface are important for the H-point phonon of Mo, this particular case was studied extensively and grids of up to 196 points in the phonon IBZ were tested.

Since it has certain desirable features, we have also studied the $\vec{k}$-point sampling method described in Ref. 58. In this method, the IBZ is divided into a number of large tetrahedrons (up to 96 in the phonon IBZ have been tested) with the center of mass of each tetrahedron serving as a point on the $\vec{k}$-point grid. Upon each iteration the energy eigenvalues at the sample grid points are fit with an empirical tight-binding (TB) method (the typical rms error of the fits are less than 0.05 eV). The weight of a state is then represented by the occupied volume of the large tetrahedron. An accurate volume is obtained by dividing each of the large tetrahedrons into 64 smaller ones and obtaining the energy eigenvalues at the corners of the small tetrahedrons using the TB fit. Linear interpolation of the bands inside the small tetrahedrons is accurate and the occupied volume can be obtained analytically.[13,59] The phonon frequency is then determined by comparing the distortion energies between two neighboring phonon displacements. The displacements must be larger than for the Gaussian technique since for very small displacements this method has a systematic error (from band crossings) which cause the total energy to deviate from the bulk or undistorted result. For this reason and because the TB method is more involved, we used the Gaussian technique for the calculations in this paper; however, in some circumstances where it is desired to have an accurate density of states (via the tetrahedron method[13,59]) or an interpolation of the first-principles eigenvalues, then the TB method might be considered.

In the iterations towards self-consistency, the dielectric matrix scheme[60] has been used to accelerate the convergence of the calculations. Self-consistency within 10^{-4} Ry on the Fourier components of the electronic potential can be achieved in four to five iterations for a typical run.

III. RESULTS

In addition to the total energy at each lattice distortion the results of our calculations yield other important quantities such as the band structure and charge density for every lattice configuration. This is an enormous amount of information and in this section we limit our presentation to just the "data" relevant for gaining a basic understanding of the electronic response for the phonons studied. Further analysis of the results and discussion is given in Sec. IV.

A. Total energy

The calculated total energies for Mo, Nb, and Zr as a function of lattice displacement corresponding to the $L(\frac{2}{3},\frac{2}{3},\frac{2}{3})$ mode are shown in Fig. 3. The curves for Mo and Nb are close to parabolic and indicate nearly harmonic behavior for small displacements. The frequencies, obtained from analysis of the curvature near zero displacement, are 6.1 and 3.6 THz for Mo and Nb, respectively. These compare well with measured values of 6.31 ± 0.04 and 3.57 ± 0.06 THz from inelastic neutron-scattering experiments.[61,46] The anharmonic components of the

TABLE I. Convergence of the frequency of the $L(\frac{2}{3},\frac{2}{3},\frac{2}{3})$ phonon in Nb as the number of $\vec{k}$ points in the sampling grid of the phonon IBZ and the value of the Gaussian smearing width (δ) used in the Fermi-surface weighting are varied.

	Phonon frequency (THz)		
	$\delta=0.025$ eV	$\delta=0.05$ eV	$\delta=0.1$ eV
20 $\vec{k}$ points (20)[a]	3.36	3.63	3.61
57 $\vec{k}$ points (55)	3.57	3.61	3.63
124 $\vec{k}$ points (112)	3.63	3.56	3.57

[a]Numbers in parentheses denote the corresponding number of grid points in the bcc IBZ.

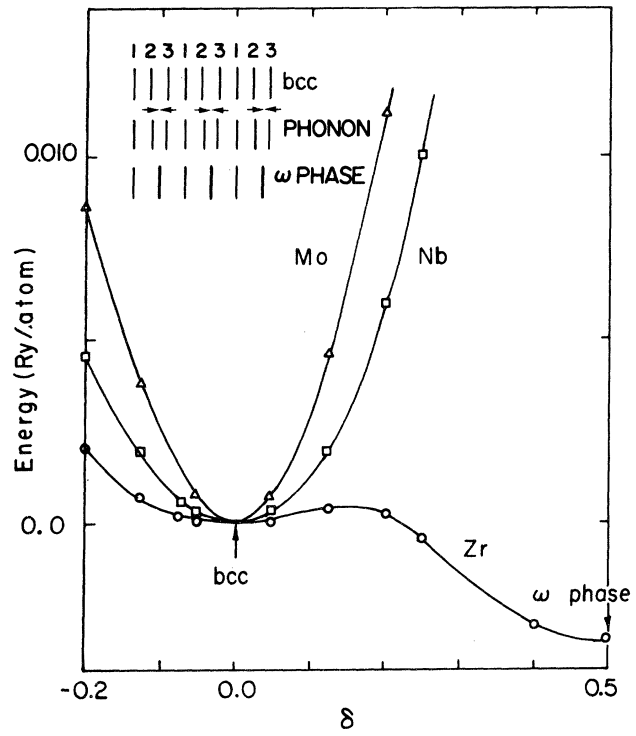

FIG. 3. Calculated total energy as a function of the displacement corresponding to the $L(\frac{2}{3},\frac{2}{3},\frac{2}{3})$ phonon for Mo, Nb, and bcc Zr. Inset shows the displacement pattern for the (111) planes of the bcc crystal. Planes 2 and 3 coincide for the ω phase.

energy-versus-displacement curves are displayed more clearly in Fig. 4 where the harmonic contribution has been divided out. It is interesting to note that while the potential well for Mo softens with increasing displacement, Nb behaves oppositely. Experimentally, the frequency of the $L(\frac{2}{3},\frac{2}{3},\frac{2}{3})$ mode in Mo softens rapidly with increasing temperature while that of Nb is relatively temperature independent. Our results suggest that in Mo the effect of anharmonicity enhances the phonon softening produced by thermal expansion of the lattice, while in Nb the effects of anharmonicity and thermal expansion counterbalance each other. Of particular interest is the curve we calcalculated for bcc, Zr, also shown in Fig. 3. The calculated potential well is strongly anharmonic; moreover, the minimum in energy does not occur at the bcc phase but rather it occurs when two of the bcc (111) planes in the unit cell collapse together to form the ω phase. We obtain an energy difference of 0.045 eV (or 520 K) per atom between these two phases. There is some uncertainty in the energy difference because we have assumed no core relaxation by using a pseudopotential and have kept an ideal C/A ratio for the ω phase. It should also be noted that temperature effects have not been included in the calculations. The stability of the bcc phase at high temperature is thought to be due to either its higher lattice vibrational entropy[62] or else the temperature dependence of the strong third-order (anharmonic) term in the potential.[63] The tendency of the bcc phase towards the formation of the ω phase at low temperature is discussed further in the next section.

The total energy-versus-displacement curves for the H-point phonons of Nb and Mo do not have a third-order term (by symmetry). The harmonic part of the curve for Nb yields a frequency of 6.4 THz which compares well with the 6.49 ± 0.10 THz from experiment.[46] On the other hand, the calculated frequency for the H-point phonon of Mo was 5.0 THz which is 9% less than the measured value of 5.51 ± 0.05 THz.[45,61] This discrepancy for Mo is larger than we would expect from the numerical precision of the calculations and the quoted experimental uncertainty. Detailed study of the discrepancy has led us to believe it is due to renormalization effects on the electronic states near the Fermi level. The renormalization is a many-body effect caused by the excitation of virtual phonons and is not included in the frozen-phonon calculations which assume the electrons move among a lattice of static (frozen) ions. The effect is significant only when nesting features on the Fermi surface allow electrons within a few $\hbar\omega_{\text{Debye}}$ of the Fermi energy to contribute strongly to the electronic screening, as is the case for a Kohn anomaly in the phonon spectrum. In such cases, the frozen-phonon results would tend to overemphasize the dip in the phonon dispersion curve. A complete analysis of this effect is contained in a separate paper.[44] The calculated phonon frequencies for the H-point and $L(\frac{2}{3},\frac{2}{3},\frac{2}{3})$ phonons of Mo and Nb along with the experimental values[46,61] are summarized in Table II.

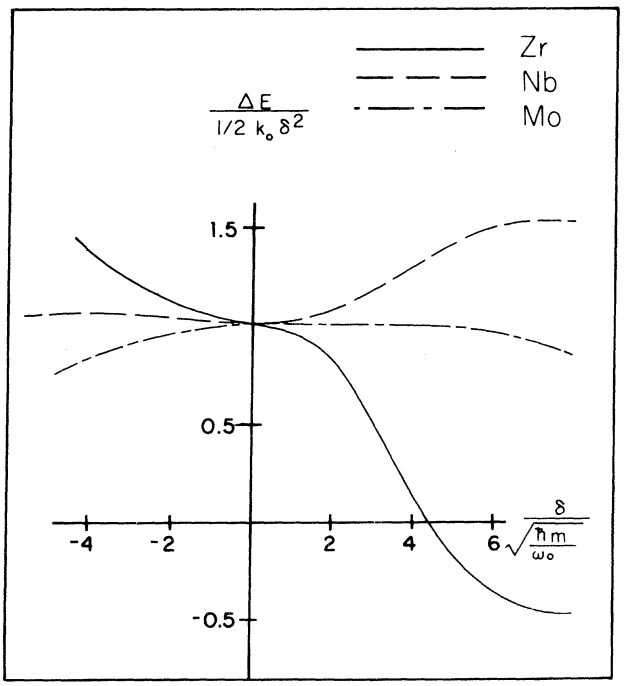

FIG. 4. Total-energy curves of Fig. 3 with the energy scaled by the different harmonic contributions to illustrate the nonharmonic character of the energy changes for displacements about equilibrium.

TABLE II. Comparison of the calculated and measured values for the frequencies of the L($\frac{2}{3},\frac{2}{3},\frac{2}{3}$) phonon and the H-point phonon in Mo and Nb. Calculated frequencies in this table are obtained from the curvatures of the energy-displacement curves at small displacements about the bcc position. We also made estimates using both an Einstein model in which a single particle vibrates in the slightly nonparabolic wells (these results are quoted in Ref. 5) and a Hellmann-Feynman force analysis (see Ref. 6). The various estimated values differ typically by ±0.1 THz.

	Mo		Nb	
	Expt.	Calc.	Expt.	Calc.
Phonon frequency (THz)				
L($\frac{2}{3},\frac{2}{3},\frac{2}{3}$)	6.31±0.04[a]	6.1	3.57±0.06[b]	3.6
H point	5.51±0.05[a]	5.0	6.49±0.10[b]	6.4

[a]Reference 61. This value was measured at 10.5 K.
[b]Reference 46.

B. Charge density

In view of the charge-fluctuation models[20,22,23] we have made an angular (l,m) decomposition of our calculated charge-density deformations about each of the atoms in the phonon-distorted lattice. According to these models the monopolar fluctuations are important for longitudinal phonons away from the zone boundary. Figure 5 shows the change with small displacement of the monopolar or spherical charge density (ρ_{00}) for the L($\frac{2}{3},\frac{2}{3},\frac{2}{3}$) phonons of Mo, Nb, and Zr. In this figure $\Delta\rho$ is defined as

$$\Delta\rho(r)=\rho_{00}^{\text{phonon}}(r)-\rho_{00}^{\text{bulk}}(r)\ , \tag{4}$$

and ρ_{00} of the jth atom is given by

$$\rho_{00}(r)=\sum_{\vec{G}}\rho(\vec{G})j_0(Gr)e^{i\vec{G}\cdot\vec{\tau}_j}\ , \tag{5}$$

where $\rho(\vec{G})$ is the component of charge density in reciprocal space, $j_0(x)$ is the spherical Bessel function of zero order, and $\vec{\tau}$ denotes the atomic position vector.

For small displacements about the bcc equilibrium position the charge-density fluctuations are similar in magnitude but very different in character; the $\Delta\rho$ curves for Nb and Zr (Fig. 5) indicate a transfer of d-like density from atoms in plane 1 to d-like density on the equivalent atoms in planes 2 and 3, whereas the $\Delta\rho$ curves for Mo show that there is a transfer of s-p—like charge about atoms in plane 1 to more d-like charge about atoms in planes 2 and 3. For Nb and Mo the charge-transfer character remains the same for large displacements, while for Zr a transfer of d-like charge from plane 1 to s-p—like charge in planes 2 and 3 develops (Fig. 6), accompanied by a decrease in the kinetic energy—just the direct opposite of the charge-transfer character for Mo. In the ω phase of Zr, 0.14 e/at. in plane 1 are transferred to planes 2 and 3, an amount which may be detectable experimentally, although the different character of the charge transferred may prevent a simple analysis of experimental results. A measurement of the electric field gradient in the ω phase suggested no charge transfer; however, this conclusion was based on comparison with lattice sums of point charges.[52] The parallel conclusion that the valence appropriate for the ω-

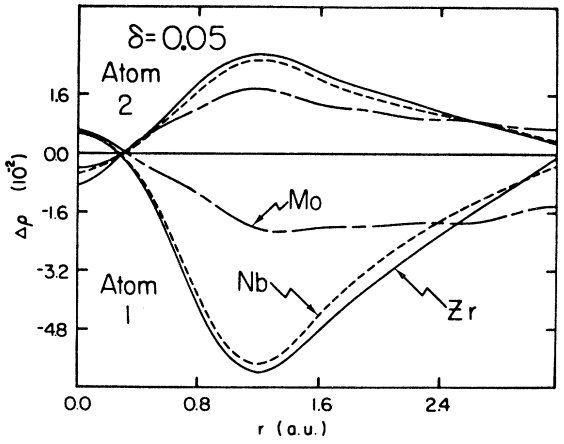

FIG. 5. Spherical component of the charge-density differences $\Delta\rho(r)=\rho_{00}^{\text{phonon}}(r)-\rho_{00}^{\text{bulk}}(r)$ for a small displacement ($\delta=0.5$ for a full displacement to the ω phase). By symmetry, atoms in plane 3 are equivalent with those in plane 2. The charge density has been multiplied by the unit-cell volume.

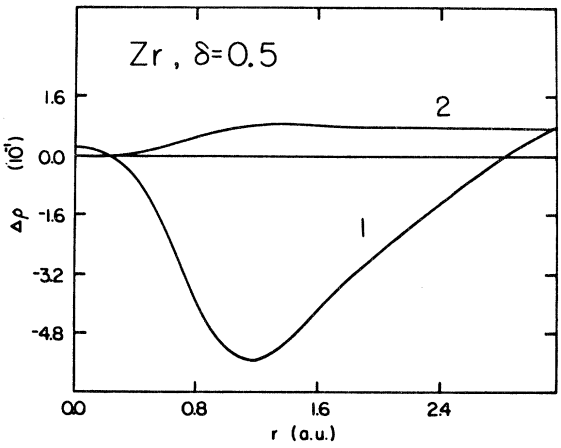

FIG. 6. Similar to Fig. 5 showing the character of the charge fluctuation for Zr with a displacement corresponding to the ω phase. Charge is transferred from atoms in plane 1 to atoms in planes 2 and 3.

phase Zr ions is +3 is also contrary to our results and probably due to the oversimplified point-charge model.

The nonspherical part of the charge density is best visualized with contour plots. Figure 7 shows a side view of the planes perpendicular to the (111) direction in the bcc crystal. The planes are labeled according to the scheme of Fig. 2 with the directions of the atomic displacements toward the ω phase indicated by arrows. From this figure it can be seen that the interatomic distances for neighboring atoms along the (111) direction remain fixed for the $L(\frac{2}{3},\frac{2}{3},\frac{2}{3})$ phonon. Thus one may think of this phonon as a shear motion of chains running along the (111) axis. In fact the $L(\frac{2}{3},\frac{2}{3},\frac{2}{3})$ phonon is not in the IBZ and could be labeled as a transverse phonon on the zone boundary at $(\frac{2}{3},-\frac{1}{3},-\frac{1}{3})$ between the P and H points. We will continue to use the conventional nomenclature. Contour plots of the valence charge density in this plane for three different displacements are shown in Figs. 8–10. We only show the densities for Mo and Zr since these metals display opposite extremes in the $L(\frac{2}{3},\frac{2}{3},\frac{2}{3})$ phonon frequency. The frequency of this phonon for Nb falls between those of Mo and Zr and the charge density is similarly "in between." The Nb frequency is "normal" in the sense that most simple bcc metals have a dip in their phonon dispersion curves similar to that of Nb near the $(\frac{2}{3},\frac{2}{3},\frac{2}{3})$ point; thus the $L(\frac{2}{3},\frac{2}{3},\frac{2}{3})$ phonon in both Mo and Zr may be considered anomalous. With small displacements (Fig. 8), the charge density for Mo shows strong d lobes giving a clear density maxima between neighboring atoms. For large displacements (Fig. 9), two main features are discernible. Firstly, the d lobes in Mo (unlike Zr) do not show appreciable change in their orientation, which indicates the d states in Mo maintain a strong interchain coupling. Secondly, overlap of d-like states has developed in Mo between nearest-neighbor atoms in planes 2 and 3, whereas for Zr the charge tends to spread into the interstitial region as the atoms are brought closer. The second feature becomes more prominent for the ω-phase configuration (Fig. 10). This delocalization is evident in the monopolar charge-fluctuation plot of Fig. 6 where d-like charge in plane 1 is transferred to s-p—like charge in planes 2 and 3. The completely opposite behavior in the charge-density response of Zr and Mo suggests that Zr is able to stabilize the ω phase by delocalizing the charge in the high-density plane (nearest-neighbor distances are now $0.817a$ in this plane compared with the $0.866a$ of the bcc lattice, where a is the bcc lattice constant). This result contradicts the model proposed by Doherty and Gibbons who suggested the stability of the ω phase was due to the development of strongly localized s—d bonds in the collapsed 2-3 plane.[64]

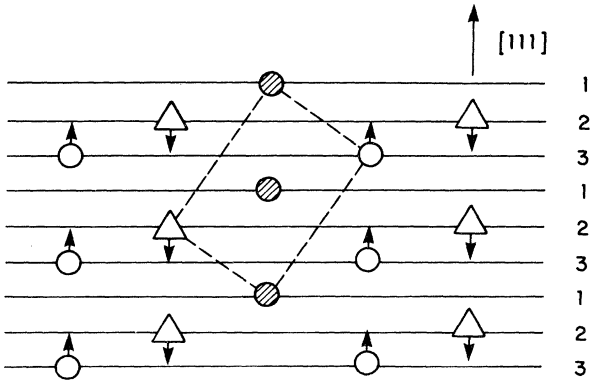

FIG. 7. Atomic displacements corresponding to the $L(\frac{2}{3},\frac{2}{3},\frac{2}{3})$ phonon in the cubic (110) plane of the bcc lattice. Shaded circles, triangles, and circles represent atoms in planes 1, 2, and 3, respectively. Dotted lines outline the diagonal plane of the bcc cubic unit cell and arrows indicate the directions of atomic displacements associated with the distortion caused by the $L(\frac{2}{2},\frac{2}{3},\frac{2}{3})$ phonon.

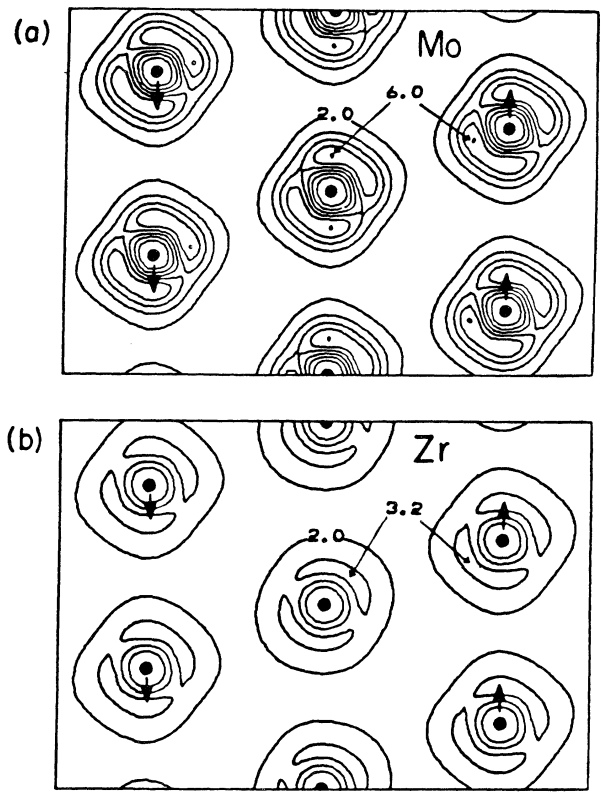

FIG. 8. Contour plots of the valence charge density for (a) Mo, and (b) Zr in the cubic (110) plane, where atoms in planes 2 and 3 have been displaced by an amount $\delta=0.05$ ($\delta=0.5$ for a full displacement to the ω phase). Solid circles denote the atomic positions and arrows denote the directions of atomic displacements.

C. H-point phonon

The sharp dip at point H in the phonon dispersion curve of Mo has been related to nesting features of the Fermi surface,[25,45,65] and a charge-density analysis is less informative. Measurements of the Mo phonon dispersion curves as a function of temperature show that the H-point anomaly diminishes at high temperature indicating the importance of states near the Fermi level in contributing to the dip.[61] Plots of the distorted Mo band structure for displacements corresponding to this phonon confirm that a large band splitting occurs at the Fermi level between

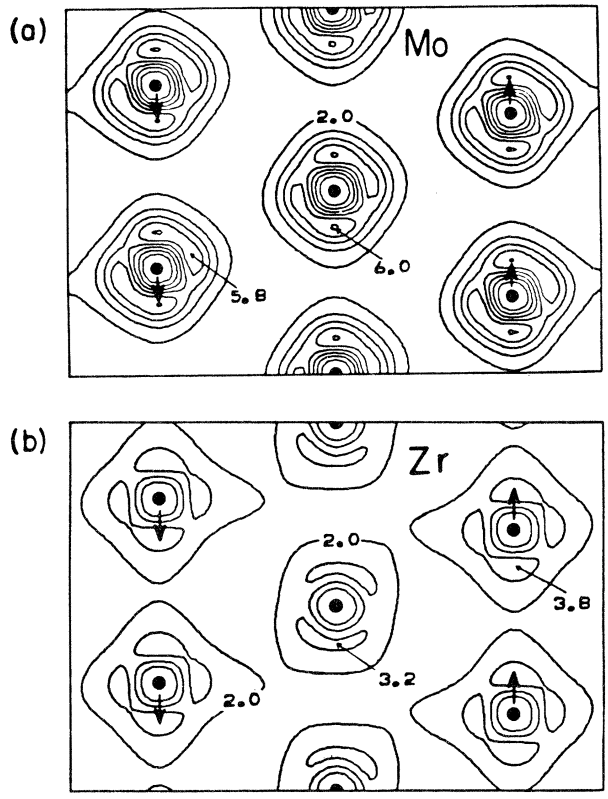

FIG. 9. Similar to Fig. 8 showing the contour plots of the valence charge density for (a) Mo, and (b) Zr in the cubic (110) plane, where atoms in planes 2 and 3 have been displaced by an amount $\delta=0.25$

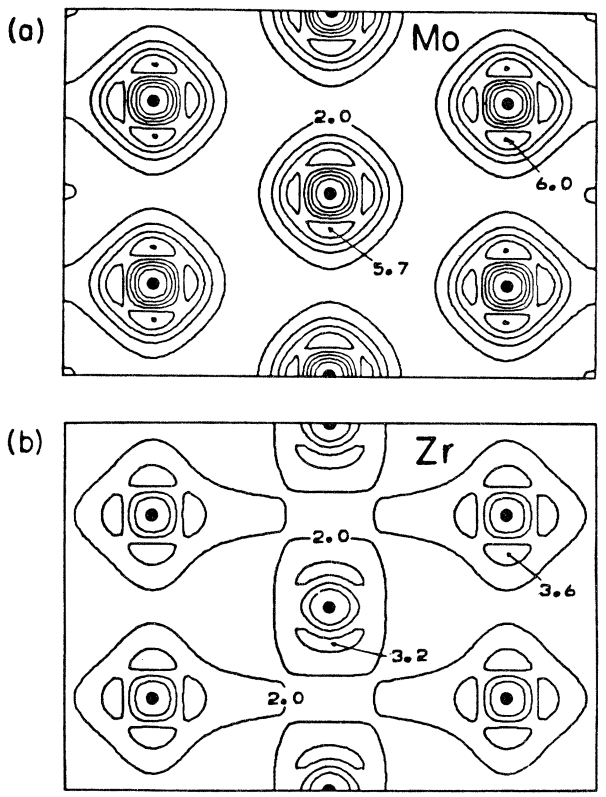

FIG. 10. Similar to Fig. 8 showing the contour plots of valence charge density for (a) Mo and (b) Zr in the cubic (110) plane, with a displacement corresponding to the ω phase.

bands with large and oppositely directed Fermi velocities. This is shown in Fig. 11. In this figure the solid lines represent the band dispersion for the bcc crystal along the k_z direction with $(k_x,k_y)=(\frac{1}{8},\frac{1}{24})2\pi/a$, and the dotted lines are the corresponding band structure for the distorted crystal with a displacement of 1.5% of the lattice constant. Note that with the phonon present the unit cell now contains two atoms and the bcc Brillouin zone is "folded" into one-half of its original volume. With a displacement of this magnitude, the total energy changes by $\sim$0.01 eV/atom while the band splitting is larger than 0.5 eV. Furthermore, for this wave vector the splitting occurs over a large volume of the Brillouin zone and significantly lowers the total energy of the crystal by lowering the energy of the occupied bands and raising the energy of the unoccupied bands. This accounts for the dip in the phonon dispersion curve. The large volume of the Brillouin zone affected and the size of the splitting for modest displacements allows convergence of total-energy calculations with a reasonable number of $\vec{k}$ points ($\sim$75 in the IBZ) using the Gaussian smearing scheme. The validity of the adiabatic approximation has been questioned for phonons such as this which involve a large Fermi-surface nesting.[66,67] We have studied this approximation and found it to make less than a 0.01-THz difference for the H-point phonon of Mo. The details of this study are contained in Ref. 44.

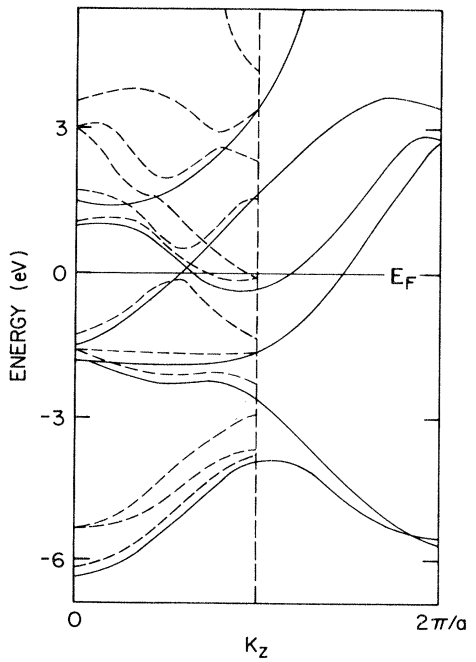

FIG. 11. Band structures along the k_z direction, with $(k_x,k_y)=(\frac{1}{8},\frac{1}{24})2\pi/a$, for the bcc lattice (solid lines) and the phonon-distorted lattice (dotted lines) associated with the distortion caused by the Mo H-point phonon.

IV. DISCUSSION

A. ω phase

Certainly one of the most interesting results of this work is the total-energy curve for Zr (Fig. 3) showing the small *(but finite)* restoring force for small displacements about the bcc phase and the stability of the ω phase relative to the bcc phase at low temperatures. Because the bcc—to—ω-phase transition is an important transition affecting mechanical and superconducting properties there have been numerous studies of the ω phase in alloys of the group-IV*B* metals (see Ref. 48 for a review). Many phenomenological theories for the ω-phase transformation have been proposed;[68] however, there does not seem to be any one model which explains all the data. A recent study found the ω phase formed in the NiAl system and critically compared the various competing models, finally deciding that only trapping of the $L(\frac{2}{3},\frac{2}{3},\frac{2}{3})$ phonons by point defects could explain the results.[69] This explanation is questionable for single-crystal bcc Zr since the results of Stassis *et al.*[47] showed that at higher temperatures, with presumably more vacancies to act as trapping sites, the quasielastic peak corresponding to the ω phase diminished greatly, unlike the temperature behavior in NiAl.[69] It seems to us that there is indeed a likelihood for the ω-phase properties of alloys to be greatly influenced by pinning sites (Stassis *et al.* did observe greater ω-phase quasielastic scattering for increased oxygen impurities), but the fact that clean hcp Zr (and Ti) forms in the pure ω phase under high pressure[49,50] and its bcc phase exhibits a huge dip for the $L(\frac{2}{3},\frac{2}{3},\frac{2}{3})$ phonon suggests the ω-phase instability is intrinsic to the bcc phase of the group-IV*B* elements (and probably to the bcc phase of the group-III*B* elements also[51]). Our calculations confirm that the instability is intrinsic and caused by electronic structure effects.[70] Our calculations also suggest the bcc—to—ω-phase transition is weakly first order since the small bump in the total-energy curve between the bcc and the ω phase will likely cause the order parameter (the atomic displacements) to jump discontinuously during the transition. Our calculations are, however, only valid for $T=0$, so there is still some question as to the nature of the transition. A related question has to do with what mechanism stabilizes the bcc phase at high temperatures. We believe that the most likely explanation involves the larger vibrational entropy (from low-lying modes) of the bcc phase;[62] however the phonon dispersion for the ω phase has not been measured and would be required to confirm this. To explain the drop in specific heat at the hcp-to-bcc transition the phonon spectrum for the bcc phase would also seem to require some phonon modes at higher energy than in the hcp phase.[71] A different view of the transition to the bcc phase has been suggested by the work of de Fontaine and Buck who developed a simple model for the interactions in the ω phase and then used Monte Carlo simulation of the dynamics at high temperatures to show the change in the average configuration from the ω to the bcc phase.[72] Another question concerns the importance of anharmonic effects involving the $L(\frac{2}{3},\frac{2}{3},\frac{2}{3})$ phonon. These are expected to be large because of the very low frequency and the uniqueness of this phonon in coupling via phonon-phonon interactions to itself in third order $(\vec{q}_\omega+\vec{q}_\omega+\vec{q}_\omega=\vec{G})$.[63] These are clearly interesting questions having to do with details of the temperature dependence of the microscopic mechanisms driving phase transitions—a topic starting to be addressed by first principles.

The electronic structure of the ω phase has been calculated previously using the augmented-plane-wave method.[50] These calculations were not self-consistent, and, we believe, did not use a sufficient number of basis functions for adequate convergence. These calculations placed the Fermi level at a peak in the density of states (DOS) with $N(E_F)=23.8$ states/Ry atom. Our DOS for the ω phase is shown in Fig. 12. It is similar to the DOS for hcp Zr,[73] and places the Fermi level near a valley with $N(E_F)=9.8$ states/Ry atom. Specific-heat measurements at low temperature would certainly distinguish between these two values. The DOS for the corresponding bcc phase of Zr is very similar to that reported by Myron *et al.*,[70] although our $N(E_F)=16.5$ states/Ry atom is smaller than the 18.2 states/Ry atom of Ref. 70 since our lattice constant was smaller and the bandwidth was therefore wider.

B. Analysis of the $L(\frac{2}{3},\frac{2}{3},\frac{2}{3})$ phonon

The predicted bcc—to—ω-phase instability in Zr and the accurate first-principles determination of phonon frequencies are definite successes of the frozen-phonon method; however, from a pedagogic viewpoint, we still have not explained the vastly different frequencies for the $L(\frac{2}{3},\frac{2}{3},\frac{2}{3})$ phonon. An analysis giving the distortion dependence of the various terms in the expression for the total energy (i.e., the kinetic, and electron-electron, the electron-ion, the ion-ion, and the exchange-correlation energies) does not seem very enlightening to us since the total energy depends on a very delicate cancellation between these large contributions. For example in Figs. 13 and 14 we show how the "pseudokinetic" energy and the electrostatic energy change with the $L(\frac{2}{3},\frac{2}{3},\frac{2}{3})$ distortion. The cancella-

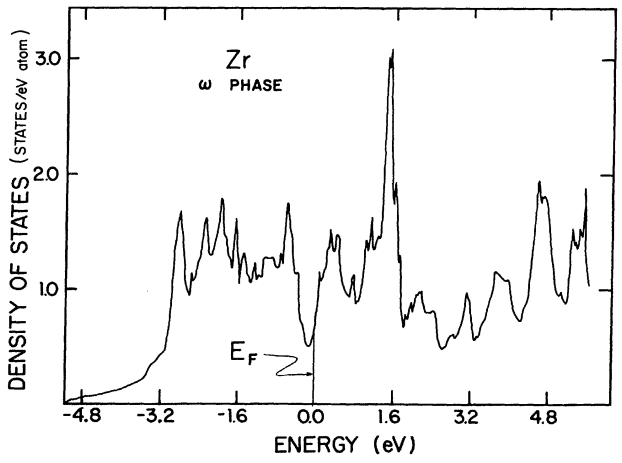

FIG. 12. Electronic density of states for the ω phase of Zr.

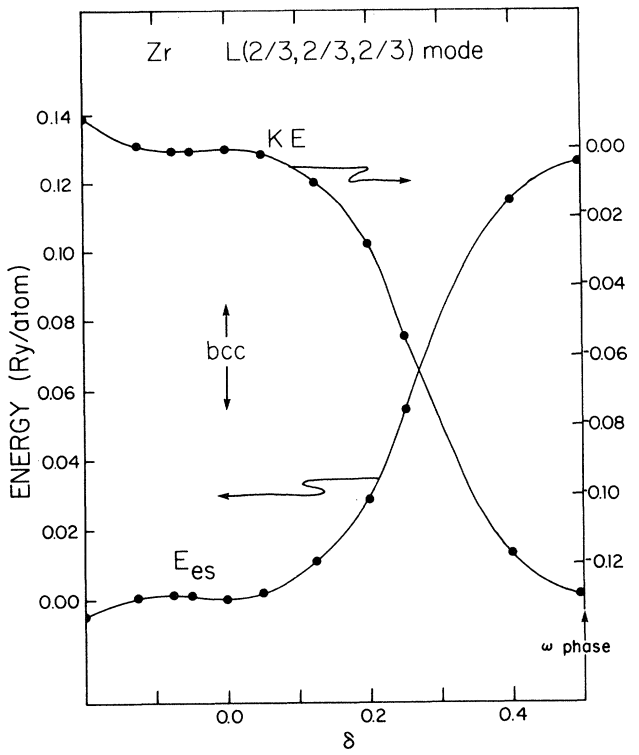

FIG. 13. Kinetic energy and electrostatic energy for the $L(\frac{2}{3},\frac{2}{3},\frac{2}{3})$ distortions of Zr. Energies are given relative to their values for the bcc phase. Also note that these quantities are for the pseudowave functions and do not represent the actual kinetic or electrostatic energy for the valence electrons in the real crystal.

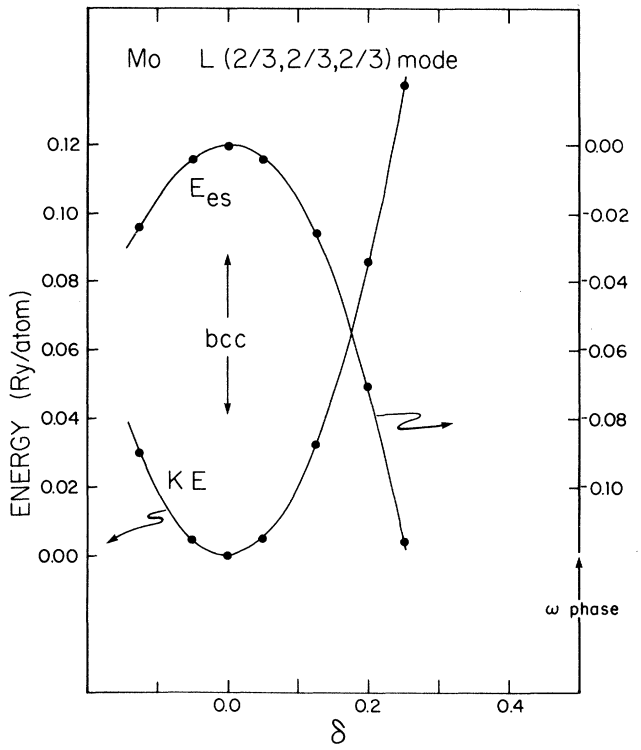

FIG. 14. Kinetic energy and electrostatic energy for the $L(\frac{2}{3},\frac{2}{3},\frac{2}{3})$ distortions of Mo. See Fig. 13.

tion between these terms results in small changes in the total energy (compare the energy scale with the one in Fig. 3). We note that the lowering of the pseudokinetic energy for the displacements toward the ω phase of Zr corresponds to the increased *s-p* character in the charge density and is opposite to the behavior seen in Mo as already discussed. The charge-fluctuation models which have been proposed are also of limited value. In order to treat the change in character of the fluctuating charge indicated by our calculations, the models would have to become more sophisticated and would have to treat the kinetic-energy changes more accurately if the correct potential-energy—kinetic-energy cancellation is to be achieved.

Although a truly simple and heuristic model may be forthcoming for transition-metal lattice dynamics we have, for now, pursued a different approach. Since we have the wave functions available for the distorted lattice, it is possible by using the Hellmann-Feynman theorem[74] to obtain the contribution of each electronic state to the interatomic forces. The details of such an analysis are described in a separate publication.[6] We briefly summarize below the essential results.

The systematic development of the dip in the longitudinal phonon branch about the $(\frac{2}{3},\frac{2}{3},\frac{2}{3})$ position as the number of valence electrons decreases (Mo to Nb to Zr) suggests that this anomaly is not associated with a sharp feature of a particular Fermi surface. Independent of any model one would expect a relative decrease of the phonon frequencies of L[111] branch in the vicinity of the $(\frac{2}{3},\frac{2}{3},\frac{2}{3})$ position for any monatomic bcc crystal,[75] since for this vibrational mode the nearest-neighbor distance between atoms in the [111] direction is preserved (illustrated in Fig. 7). Thus the corresponding restoring force vanishes, and, as previously mentioned, the atomic displacements for this mode can be viewed as a shearing motion between chains of atoms along the [111] direction. In view of the above discussion, the absence of the dip in Mo (also in isoelectronic Cr and W) must be due to some special aspects of the electronic structure. The increase in the frequency of the $L(\frac{2}{3},\frac{2}{3},\frac{2}{3})$ phonon as one goes from Zr to Mo is accompanied by an increase in the bonding *d*-like charge density directed along the nearest-neighbor (111) direction[76] of the bcc lattice. Using the Hellmann-Feynman force analysis we have determined that the increased frequency of this phonon for Mo over Nb is caused by the development of directional bonding from the additional occupied *d* states. This gives rise to bond-bending forces which help to restore the equilibrium position much like the situation in covalently bonded semiconductors. This is opposite to the behavior of simple metals where free-electron screening merely acts to reduce the ionic restoring forces. Similar analysis for Zr revealed the *d* electrons along the (111) chains moved almost rigidly with the displaced ions. Since these *d* states are more lo-

calized than free-electron orbitals, the screening is more effective than for simple metals. The transition to the ω phase involves large displacements, and, through a force analysis, the driving mechanism was traced to shifts of the band structure near the Fermi level.[6] These shifts in band occupation result in the change in charge density already discussed.

V. CONCLUSION

The calculations presented in this paper represent a new and potentially very powerful first-principles tool for the study of interatomic interactions in solids. They demonstrate that the phonon frequencies of transition metals can be accurately calculated using the frozen-phonon method with the only required input being the atomic numbers and masses. The accuracy of the results suggests that the use of the local-density-functional theory and the frozen-core approximation are adequate for meaningful calculations. In addition, the method has the distinct advantage over other approaches to lattice dynamics in that the displacements of the nuclei about their equilibrium position need not be small. Thus the microscopic mechanisms governing structural phase transitions can be studied in much greater detail than previously.

ACKNOWLEDGMENTS

We would like to thank Dr. S. H. Liu and Dr. W. Weber for their interest and encouragement, and Professor C. Stassis for many stimulating discussions. Ames Laboratory is operated for the U.S. Department of Energy by Iowa State University under Contract No. W-7405-Eng-82. This work was supported by the Director for Energy Research, Office of Basic Energy Sciences.

[1]G. Grimvall, in *Ab Initio Calculation of Phonon Spectra,* edited by J. T. Devreese, V. E. Van Doren, and P. E. Van Camp (Plenum, New York, 1983), p. 117.

[2]E. G. Brovman and Y. M. Kagan, in *Dynamical Properties of Solids,* edited by G. K. Horton and A. A. Maradudin (North-Holland, Amsterdam, 1974), Vol. I.

[3]S. K. Sinha, in *Dynamical Properties in Solids,* edited by G. K. Horton and A. A. Maradudin (North-Holland, Amsterdam, 1979), Vol. III, p. 1.

[4]J. Ashkenazi and M. Dacorogna, in *Ab Initio Calculation of Phonon Spectra,* Ref. 1, p. 181.

[5]K.-M. Ho, C.-L. Fu, B. N. Harmon, W. Weber, and D. R. Hamann, Phys. Rev. Lett. 49, 673 (1982); K.-M. Ho, C.-L. Fu, and B. N. Harmon, in *Superconductivity in d- and f-Band Transition Metals,* edited by W. Buckel and W. Weber (Kernforschungszentrum, Karlsruhe GmbH, Karlsruhe, W. Germany, 1982), p. 511.

[6]K.-M. Ho, C.-L. Fu, and B. N. Harmon, Phys. Rev. B 28, 6687 (1983).

[7]M. Born and K. Huang, *Dynamical Theory of Crystal Lattice* (Oxford University Press, London, 1956).

[8]A. A. Maradudin, E. W. Montroll, G. H. Weiss, and I. P. Ipatova, *Theory of Lattice Dynamics in the Harmonic Approximation* (Academic, New York, 1971).

[9]G. Venkataraman, L. A. Feldkamp, and V. C. Sahni, *Dynamics of Perfect Crystals* (MIT Press, Cambridge, Mass., 1975).

[10]L. J. Sham, in *Dynamical Properties of Solids,* Ref. 2, Vol. I, p. 301.

[11]S. K. Sinha, Crit. Rev. Solid State Sci. 4, 273 (1973).

[12]P.-A. Lindgård, Solid State Commun. 16, 481 (1975).

[13]J. Rath and A. J. Freeman, Phys. Rev. B 11, 2109 (1975).

[14]S. K. Sinha, T. O. Brun, L. D. Muhlestein, and J. Sakurai, Phys. Rev. B 1, 2430 (1970).

[15]W. A. Kamitakahara, B. N. Harmon, J. G. Taylor, L. Kopp, H. R. Shanks, and J. Rath, Phys. Rev. Lett. 36, 1393 (1976).

[16]M. Gupta, and A. J. Freeman, in *Superconductivity in d- and f-Band Metals,* edited by D. H. Douglas (Plenum, New York, 1976), p. 313.

[17]B. M. Klein, D. A. Papaconstantopoulos, and L. L. Boyer, in *Superconductivity in d- and f-Band Metals,* Ref. 16, p. 339

[18]For example, see J. F. Cooke, H. L. Davis, and M. Mostoller, Phys. Rev. B 9, 1485 (1974), and Ref. 70.

[19]W. Hanke and H. Bilz, in *Neutron Inelastic Scattering* (International Atomic Energy Agency, Vienna, 1972).

[20]S. K. Sinha and B. N. Harmon, Phys. Rev. Lett. 35, 1515 (1975); in *Superconductivity in d- and f-Band Metals,* Ref. 16.

[21]W. Hanke, J. Hafner, and H. Bilz, Phys. Rev. Lett. 37, 1560 (1976).

[22]N. Wakabayashi, Solid State Commun. 23, 737 (1977).

[23]P. B. Allen, Phys. Rev. 16, 5139 (1977).

[24]I. R. Gomersall, Ph.D. thesis, University of Bristol, 1975; W. E. Pickett and B. L. Gyorffy, in *Superconductivity in d- and f-Band Metals,* Ref. 16; C. M. Varma and R. C. Dynes, *ibid.*

[25]C. M. Varma and W. Weber, Phys. Rev. Lett. 39, 1094 (1977); Phys. Rev. B 19, 6142 (1979).

[26]W. Weber, P. Rodhammer, L. Pintschovius, W. Reichardt, F. Gompf, and A. N. Christensen, Phys. Rev. Lett. 43, 868 (1979).

[27]W. Weber, in *Physics of Transition Metals 1980,* edited by P. Rhodes (Institute of Physics, Bristol, 1980).

[28]W. Weber, in *Superconductivity in d- and f-Band Metals,* Ref. 5, p. 15.

[29]P. Hohenberg and W. Kohn, Phys. Rev. 136, B864 (1964); W. Kohn and L. J. Sham, Phys. Rev. 148, A1133 (1965).

[30]M. Born and R. Oppenheimer, Ann. Phys. (Leipzig) 84, 457 (1927).

[31]M. T. Yin and M. L. Cohen, Phys. Rev. Lett. 45, 1004 (1980); Phys. Rev. B 26, 3259 (1982).

[32]K. Kunc and R. M. Martin, Phys. Rev. Lett. 48, 406 (1982).

[33]B. N. Harmon, W. Weber, and D. R. Hamann, Phys. Rev. B 25, 1109 (1982).

[34]O. H. Nielsen and R. M. Martin, Phys. Rev. Lett. 50, 697 (1983).

[35]P. K. Lam and M. L. Cohen, Phys. Rev. B 25, 6139 (1982).

[36]K. Kunc and R. M. Martin, J. Phys. (Paris) Colloq. 42, C6-649 (1981).

[37]M. T. Yin and M. L. Cohen, Phys. Rev. B 25, 4317 (1982).

[38]S. J. Gale and D. G. Pettifor, Solid State Commun. 24, 175 (1977).

[39]K. Terakura, J. Phys. C 11, 469 (1978).

[40]K. Maschke and A. Baldereschi, in *Physics of Semiconductors 1978,* edited by B. L. H. Wilson (Institute of Physics, Bristol,

1979).

[41]S. J. Gale, Ph.D. thesis, University of Cambridge, 1977, referred to by M. J. Kelly, in *Solid State Physics,* edited by H. Ehrenreich, F. Seitz, and D. Turnbull (Academic, New York, 1980), Vol. 35, p. 368.

[42]A. Baldereschi and R. Resta, in *Ab Initio Calculation of Phonon Spectra,* Ref. 1, p. 1.

[43]B. N. Harmon and K.-M. Ho, in *Superconductivity in d- and f-Band Metals,* edited by H. Suhl and M. B. Maple (Academic, New York, 1980), p. 173.

[44]C.-L. Fu, K.-M. Ho, B. N. Harmon, and S. H. Liu, Phys. Rev. B 28, 2957 (1983).

[45]B. N. Powell, P. Martel, and A. D. B. Woods, Phys. Rev. 171, 727 (1968). See Ref. 61 for low-temperature measurements.

[46]Y. Nakagawa and A. D. B. Woods, Phys. Rev. Lett. 11, 271 (1963).

[47]C. Stassis, J. Zarestky, and N. Wakabayashi, Phys. Rev. Lett. 41, 1726 (1978).

[48]B. S. Hickman, J. Mater. Sci. 4, 554 (1969); S. L. Sass, J. Less Common Met. 28, 157 (1972).

[49]A. Jayaraman, W. Klement, and G. C. Kennedy, Phys. Rev. 134, 664 (1963); J. D. Jamieson, Science 140, 72 (1963).

[50]Y. K. Vohra, S. K. Sikka, and R. Chidambaram, J. Phys. F 9, 1771 (1979).

[51]C. Stassis, J. Zarestky, C.-K. Loong, and R. N. Nicklow, Bull. Amer. Phys. Soc. 28, 379 (1983), and unpublished.

[52]E. N. Kaufmann and D. B. McWhan, Phys. Rev. B 8, 1390 (1973). See their note added in proof.

[53]D. L. Johnson, B. N. Harmon, and S. H. Liu, J. Chem. Phys. 73, 1898 (1980); S. H. Liu, L. Kopp, W. B. England, and H. W. Myron, Phys. Rev. B 11, 3463 (1975).

[54]C.-L. Fu and K.-M. Ho, Phys. Rev. B 28, 5480 (1983). This paper contains the expressions used in the calculation of the total energy as well as details of other calculational procedures used in our work.

[55]S. G. Louie, K.-M. Ho, and M. L. Cohen, Phys. Rev. B 19, 1774 (1979).

[56]D. R. Hamann, M. Schlüter, and C. Chiang, Phys. Rev. Lett. 43, 1494 (1979).

[57]L. Hedin and B. I. Lundqvist, J. Phys. C 4, 2064 (1971).

[58]B. N. Harmon, W. Weber, and D. R. Hamann, J. Phys. (Paris) Colloq. 42, C6-628 (1981).

[59]O. Jepsen and O. K. Andersen, Solid State Commun. 9, 1763 (1971).

[60]K. M. Ho, J. Ihm, and J. D. Joannopoulos, Phys. Rev. B 25, 4260 (1982).

[61]J. Zarestky, C. Stassis, B. N. Harmon, K.-M. Ho, and C.-L. Fu, Phys. Rev. B 28, 697 (1983).

[62]C. Zener, Phys. Rev. 71, 846 (1947); J. Friedel, J. Phys. Lett. (Paris) 35, L59 (1974).

[63]H. E. Cook, Acta Metall. 22, 239 (1974); 23, 1041 (1975).

[64]J. E. Doherty and D. F. Gibbons, Acta Metall. 19, 275 (1971).

[65]T. M. Rice and B. I. Halperin, Phys. Rev. B 1, 509 (1970).

[66]G. V. Chester, Adv. Phys. 10, 357 (1961).

[67]E. G. Brovman and Y. Kogan, Zh. Eksp. Teor. Fiz. 52, 557 (1967) [Soviet Phys.—JETP 25, 365 (1967)].

[68]J. M. Sanchez and D. de Fontaine, J. Phys. (Paris) Colloq. 38, C7-444 (1977).

[69]P. Georgopoulos and J. B. Cohen, Acta Metall. 29, 1535 (1981).

[70]The dip at $(\frac{2}{3},\frac{2}{3},\frac{2}{3})$ is an example of an electronic structure caused anomaly which can not be related to structure in $\chi^0(q)$. See H. W. Myron, A. J. Freeman, and S. C. Moss, Solid State Commun. 17, 1467 (1975), for the $\chi^0(q)$ of bcc Zr. Electron-phonon matrix elements are essential for producing the dip; see, for example, A. L. Simons and C. M. Varma, Solid State Commun. 35, 317 (1980).

[71]G. Grimvall, in *Transition Metals 1977,* edited by M. J. G. Lee, J. M. Perz, and E. Fawcett (Institute of Physics, Bristol, 1978).

[72]D. de Fontaine and O. Buck, Philos. Mag. 27, 967 (1973).

[73]C. Stassis, J. Zarestky, D. Arch, O. D. McMasters, and B. N. Harmon, Phys. Rev. B 18, 2632 (1978).

[74]H. Hellmann, *Einfuhrung in die Quantenchemie* (in German) (Deuticke, Leipzig, Germany, 1937); R. P. Feynman, Phys. Rev. 56, 340 (1939).

[75]C. Falter, W. Ludwig, M. Selmke, and W. Zierau, Phys. Lett. 90A, 250 (1982).

[76]K. M. Ho, S. G. Louie, J. R. Chelikowsky, and M. L. Cohen, Phys. Rev. B 15, 1755 (1977).